Journal of Catalysis 276 (2010) 351–359

Contents lists available at ScienceDirect

Journal of Catalysis

journal homepage: www.elsevier.com/locate/jcat

Designing Pt nanoparticles supported on CeO_2–Al_2O_3: Synthesis, characterization and catalytic properties in the steam reforming and partial oxidation of methane

P.J.S. Prieto [a], A.P. Ferreira [a], P.S. Haddad [b], D. Zanchet [b,c,*], J.M.C. Bueno [a,*]

[a] Department of Chemical Engineering, Federal University of São Carlos, C.P. 676, 13565-905 São Carlos, SP, Brazil
[b] Brazilian Synchrotron Light Laboratory – LNLS, C.P. 6192, 13083-970 Campinas, SP, Brazil
[c] Institute of Chemistry, University of Campinas – UNICAMP, C.P. 6154, 13083-970, Campinas, SP, Brazil

ARTICLE INFO

Article history:
Received 9 July 2010
Revised 10 September 2010
Accepted 25 September 2010
Available online 5 November 2010

Keywords:
Pt catalysts
CeO_2–Al_2O_3 carriers
Pt nanoparticles
Methane oxyforming reactions
Steam reforming of methane
Partial oxidation of methane
XAFS
FTIR

ABSTRACT

Platinum nanoparticles (Pt-NPs) of about 3 nm were synthesized by colloidal methods and encapsulated in mesoporous Al_2O_3 and CeO_2–Al_2O_3 prepared by sol–gel method. A new strategy to synthesize Pt clusters of uniform size supported on mixed oxides was achieved, and the catalysts were characterized by Fourier transform infrared spectroscopy of adsorbed CO, transmission electron microscopy and X-ray absorption fine structure spectroscopy and tested in steam reforming of methane (SRM) and partial oxidation of methane (POM). Pt-NPs were well dispersed on the supports, and there was no significant modification of their size during calcination and under POM conditions. In the SRM, the CH_4 turnover rate on the Pt-NPs/CeO_2–Al_2O_3 catalyst was twice higher than the one on the Pt-NPs/Al_2O_3 catalyst, despite their similar Pt-NP sizes. The use of colloidal Pt-NPs to produce nanocatalysts with similar particle size clearly pointed out the important role of the CeO_2 in promoting the catalytic activity.

1. Introduction

The partial oxidation, steam reforming and autothermal reforming of natural gas are among the main approaches being investigated for the production of H_2 and synthesis gas. In particular, the partial oxidation of methane (POM) and autothermal reforming of methane (ATRM) produce synthesis gas with H_2/CO ratio about 2:1, desirable for the synthesis of hydrocarbons [1]. As the POM and ATRM run at high temperatures (~1173 K or above), highly stable catalysts are required. Recently, it has been demonstrated in experimental and theoretical work that the catalytic activity for the steam reforming of methane (SRM) observed on the surface of metals (Ni, Pt, Ir and Ru) increases with the dispersion of the metal [2]. The change in activation of CH_4 depends on the kind of metal and increases with decreasing d-orbital occupancy [3].

Regarding the influence of the support on activity, Wei and Iglesia [4] reported that the support had no effect on turnover rates (TOF_{CH4}) in SRM. On the other hand, we have shown in previous studies that the stability of conventional Pd- and Pt-supported catalysts in POM and the activity in SRM depend strongly on the support [5,6]. Furthermore, changing the support in these catalysts resulted in different metal surface structures, which interacted differently with CO. In those experiments, the effects of the support and metal particle size were strongly interdependent, making it difficult to analyze the role of the support and the particle size separately.

In those studies, the catalysts were prepared by conventional techniques, such as impregnation followed by calcination/reduction, which often result in metal clusters with a wide size distribution and that usually depends on the support. It is known that the surface structure on small metal nanocrystals may vary drastically in the 1–5 nm size range and, as a consequence, their size distribution may play a critical role in structure-sensitive catalytic reactions [7]. In the case of Pt, in particular, the degree of Pt sintering also depends on the size of the Pt particles [8] and the PtO_x–oxide support interaction [9]. Therefore, it is highly desirable to design Pt catalysts with fine metal dispersion obtained in a controllable way. For this propose, the use of colloidal nanoparticles has already been proved to be a successful approach [10].

In this paper, we describe a simple method to prepare Al_2O_3- and CeO_2–Al_2O_3-supported Pt nanoparticle catalysts based on the incorporation of colloidal Pt nanoparticles (Pt-NPs) during the sol–gel preparation of the supports. By this approach, we fixed the Pt-NP size while changing the support oxide properties.

* Corresponding authors. Fax: +55 19 35213023 (D. Zanchet), +55 16 33518466 (J.M.C. Bueno).
E-mail address: jmcb@ufscar.br (J.M.C. Bueno).

0021-9517/$ - see front matter © 2010 Elsevier Inc. All rights reserved.
doi:10.1016/j.jcat.2010.09.025

Pt-NPs/Al_2O_3 and Pt-NPs/CeO_2–Al_2O_3 catalysts were tested in SRM at low temperature to clarify the effect of the support on activity. The Pt-NPs/Al_2O_3 and Pt-NPs/CeO_2–Al_2O_3 catalysts were then subjected to POM conditions at higher temperature to observe the effect of the support on stability. The samples were characterized by nitrogen adsorption–desorption isotherms, X-ray diffraction (XRD), Fourier transform infrared spectroscopy (FTIR) of adsorbed CO, transmission electron microscopy (TEM) and X-ray absorption fine structure spectroscopy at the Pt L_{III}-edge (XAFS). The density of exposed Pt sites was determined by the cyclohexane dehydrogenation reaction rate (r_{C6H6}).

2. Experimental

2.1. Catalyst preparation

The Pt-NPs were prepared by the method of Teranishi et al. [11], in which $H_2PtCl_6{\cdot}6H_2O$ (52.5 mg) was dissolved in a mixture of double-distilled water (13.5 mL) and methanol (121.5 mL) containing poly(N-vinyl-2-pyrrolidone) (PVP: 118.5 mg, MW 40,000, Aldrich). The solution was refluxed in a 250-mL flask for 3 h under air. The Pt-NPs were precipitated from the colloidal suspension by adding a large amount of diethyl ether. The precipitate was redispersed in 150 mL anhydrous methanol, giving a dark brown Pt-NPs sol that was used in the preparation of Pt-NPs-supported catalysts.

The supported Pt nanocatalysts, Pt-NPs/Al_2O_3 and Pt-NPs/CeO_2–Al_2O_3 with 12 wt% of CeO_2 were prepared by adding an appropriate volume of the dark brown solution of Pt-NPs during the Al_2O_3 or CeO_2–Al_2O_3 sol–gel synthesis. Briefly, a solution containing 4.2 g of aluminum tri-*sec*-butoxide ($Al(OC_4H_9\ sec)_3$, p.a., 99%, Merck) in 28 mL of ethanol (p.a., Merck) was prepared and maintained under vigorous stirring at 363 K. To obtain the CeO_2–Al_2O_3 sol with 12 wt% of CeO_2, 5 mL of an aqueous solution of 0.79 mmol $Ce(NO_3)_3{\cdot}6H_2O$ (99%, p.a., Aldrich) was added to the first solution. The mixtures were refluxed for 1 h at 363 K. After this period, 4.7 mL of an aqueous solution of nitric acid (0.109 mol L^{-1}, Merck, p.a.) was added to peptize the Al_2O_3 or CeO_2–Al_2O_3, and the mixtures were refluxed for 14 h. After that, the colloidal solution of Pt-NPs (150 mL) was added to the gel at a nominal Pt concentration of about 0.3 wt% in the calcined catalyst.

The gelatinous precipitates were dried for 2–3 days in air at room temperature, forming the xerogels, which were calcined at 773 K for 4 h under a flow of synthetic air. As control experiments, samples of the support without the incorporation of Pt-NPs were prepared in a similar way. Calcination at 1073 K for 24 h was also performed to evaluate the stability of the supports and catalysts. Unless indicated, the standard calcination condition was 773 K and 4 h.

2.2. Characterization

The size and structure of the Pt-NPs were probed by TEM, using a JEM 3010 microscope, operating at 300 kV (1.7 Å point resolution) at the LNLS (Brazilian Synchrotron Light Laboratory, Campinas, Brazil). TEM samples were prepared by dropping either the Pt-NPs colloidal solution or a suspension of the nanocatalysts in isopropanol on previously prepared amorphous carbon films supported on copper grids.

The chemical analyses of the Pt-NPs/Al_2O_3 and Pt-NPs/CeO_2–Al_2O_3 samples were performed by inductively coupled plasma-atomic emission spectroscopy (ICP-AES). Surface area (S_{BET}), pore volume (V_p) and average pore diameter (D_{pore}) of the catalysts were measured before reduction by N_2 adsorption–desorption isotherm at liquid nitrogen temperature, using the Micromeritics ASAP 2000 apparatus.

XRD patterns of the supports and catalysts were collected with a Rigaku DMAX 2500 PC diffractometer, using Cu Kα radiation with a Ni filter, step size of 0.020° in 2θ, and an accumulation time of 10 s per step. The apparent crystallite size of CeO_2 (D_{CeO2}) was determined by applying the Scherrer equation to the (0 2 0) peak [12].

UV–Vis absorption spectra were recorded over the range of 200–800 nm with an AGILENT 8453 UV–Vis spectrometer.

FTIR analysis of adsorbed CO was carried out with a Thermo Nicolet 4700 Nexus FTIR spectrophotometer with MCT detector and Diffuse Reflectance Infrared Fourier Transform Spectroscopy – reactor cell with CaF_2 windows (DRIFTS HTHV cell – Spectra Tech). The IR spectra were recorded using 64 scans at 4 cm^{-1} resolution. The Pt-NPs/Al_2O_3 and Pt-NPs/CeO_2–Al_2O_3 catalysts were pre-reduced at 773 K with a 1:3 mixture of H_2/N_2, flowing at 100 mL min^{-1} for 1 h. The catalyst was kept under vacuum at temperature of reduction for 5 min, after which N_2 was introduced into the cell and the samples cooled down to 298 K.

The catalysts were exposed to CO atmosphere (10 torr) at 298 K. Temperature-programmed desorption of CO (TPD-CO) experiments were performed as described in detail previously [13]. The reduced Pt-NPs/Al_2O_3 and Pt-NPs/CeO_2–Al_2O_3 samples, with CO adsorbed at 298 K, were then subjected to successive cycles of heating to various temperatures and cooling to 298 K, to collect further spectra.

The Pt dispersions in the reduced catalysts were estimated from r_{C6H6} obtained at 543 K. For that, a calibration curve was first obtained for a set of Pt–Al_2O_3 catalysts with variable dispersion correlating chemisorption data with r_{C6H6}. Then, the r_{C6H6} values for the catalysts used in this work were obtained and compared with a standard sample. Dehydrogenation of cyclohexane was performed in a fixed-bed reactor at atmospheric pressure. The procedure is described elsewhere [14].

XAFS was performed at the XAFS 2 beamline of the LNLS (Campinas, Brazil). The measurements were performed in transmission mode at the Pt L_{III}-edge (11,564 eV). Samples were prepared as pellets and placed inside a quartz tubular furnace (diameter 20 mm and X-ray path length 440 mm) with refrigerated kapton windows. To improve the signal-to-noise ratio, the content of Pt used for the XAFS analysis was 0.6 wt%. All other characterizations and catalytic tests were performed with 0.3 wt% Pt loading. The calcined samples were heated from room temperature to 773 K at 10 K min^{-1} under a flow of H_2/N_2 (5:95), held for 1 h at 773 K and then cooled down to 298 K, keeping the flow of H_2/N_2 throughout. After this thermal treatment, the extended X-ray absorption fine structure (EXAFS) spectra were collected at 298 K. The data analysis was performed using the IFEFFIT software package [15].

2.3. Catalytic test

The SRM rates were measured on catalyst powder (100 mg; 80–100 mesh particles) diluted in powdered quartz (300 mg) of similar grain size in a fixed-bed quartz reactor (i.d. 8 mm) at atmospheric pressure. The gas compositions of the reactants and products were analyzed by gas chromatography, as previously described [6]. Feed composition was 1:3:0.5 $CH_4/H_2O/N_2$, with a total flow rate of 2×10^{-2} mol min^{-1}. Before the reaction, the samples were reduced *in situ* at 773 K for 1.5 h in 10% H_2/N_2 flowing at 50 mL min^{-1}. The specific rates of the SRM reaction (r_{CH4}) were corrected for reactant depletion and approach to equilibrium, as described by Wei and Iglesia [4]. The absence of external mass and heat transfer resistances were confirmed by the calculation of partial pressures and temperature differences between bulk and surface of catalysts particle. The forward CH_4 turnover rate (TOF_{CH4}) calculations were based on r_{CH4} and the Pt dispersion. The apparent activation energies (E_{app}) were estimated by using nonlinear methods to fit the experimental data to the Arrhenius equation.

The catalytic performance under POM conditions was observed in a fixed-bed quartz reactor at atmospheric pressure. The catalyst (40 mg) was diluted with SiC (72 mg) in order to minimize heat effects. Prior to reaction, the samples were reduced *in situ* at 773 K for 1.5 h in a flow of 10%H_2/N_2 (50 mL min^{-1}) and then heated up to the reaction temperature (1073 K) flowing N_2. For this reaction, a reactant mixture of $CH_4/O_2/N_2$ in the ratio 2:1:1 was passed through the reactor, at a flow rate of 150 mL min^{-1}. The stability of the catalysts was tested by performing the reaction at 1073 K for 24 h on stream. The products were analyzed on-line by a VARIAN 3800 gas chromatograph.

3. Results

Fig. 1a and b presents a TEM image and corresponding histogram of Pt-NPs used to produce the nanocatalysts, showing a mean diameter of 3.2 nm and standard deviation σ = 15%. Fig. 1c–f shows TEM images of the fresh Pt-NPs/Al_2O_3 (c and e) and Pt-NPs/CeO_2–

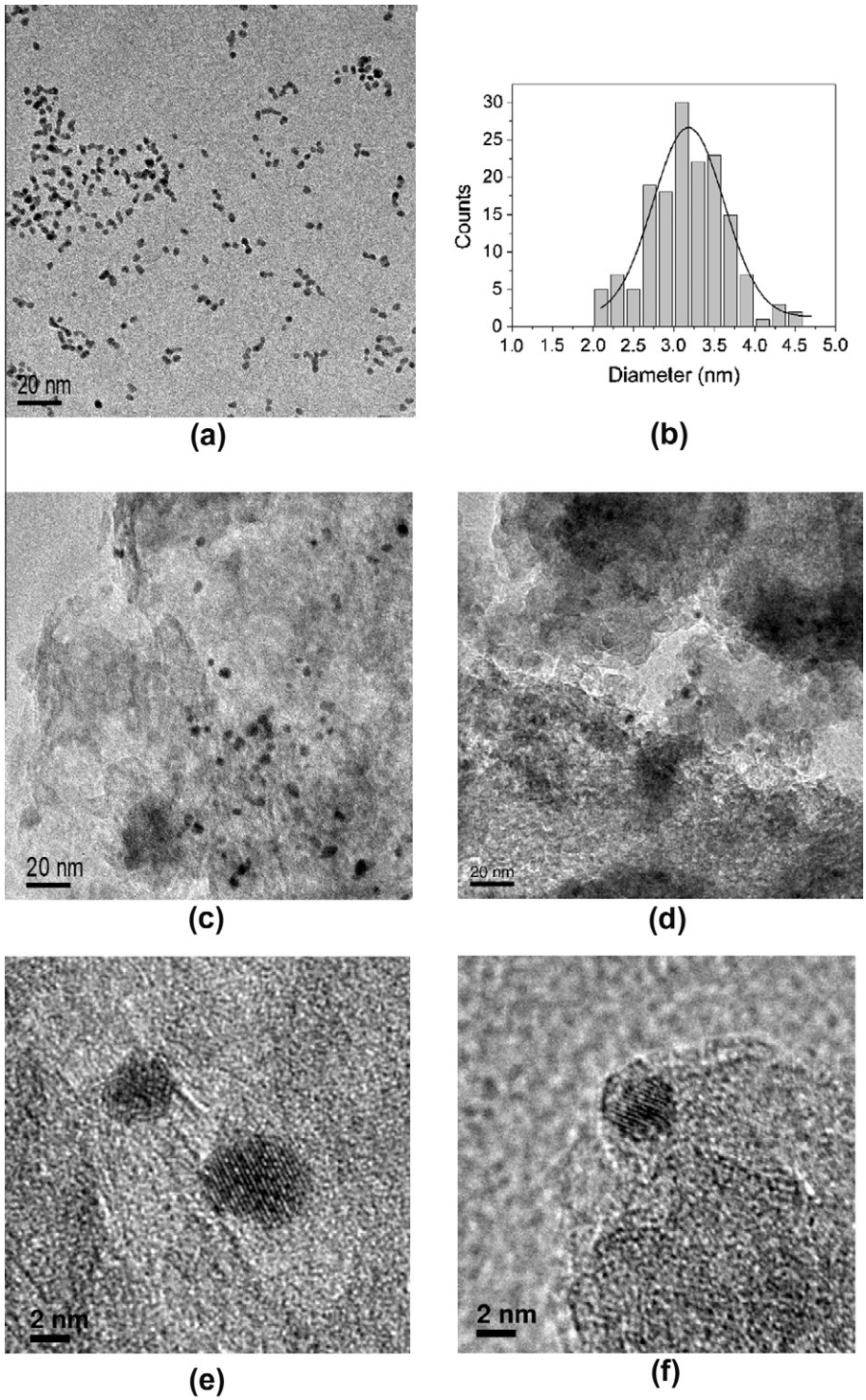

Fig. 1. (a) TEM image of the colloidal Pt-NPs and (b) corresponding histogram (mean size = 3.2 nm, σ = 15%). TEM images of (c and e) Pt-NPs/Al_2O_3 and (d and f) Pt-NPs/CeO_2–Al_2O_3 fresh catalysts.

Table 1
Chemical analysis, S_{BET}, V_p and D_{pore} of Pt–Al_2O_3 and Pt/CeO_2–Al_2O_3 catalysts. D_{CeO2} obtained by XRD is also shown for the Pt/CeO_2–Al_2O_3 sample.

Sample	CeO_2 (wt%)	Pt (wt%)	S_{BET} ($m^2\ g^{-1}$)	V_p ($cm^3\ g^{-1}$)	D_{pore} (nm)	D_{CeO2} (nm)
Pt-NPs/Al_2O_3	–	0.32	304	0.29	3.6	–
Pt-NPs/CeO_2–Al_2O_3	11.2	0.38	203	0.16	3.2	4.8 (7.3)[a]

[a] Samples calcined in air at 1073 K.

Al_2O_3 (d and f) catalysts (after calcination at 773 K), indicating that the Pt-NPs remain isolated during gel formation and after calcination.

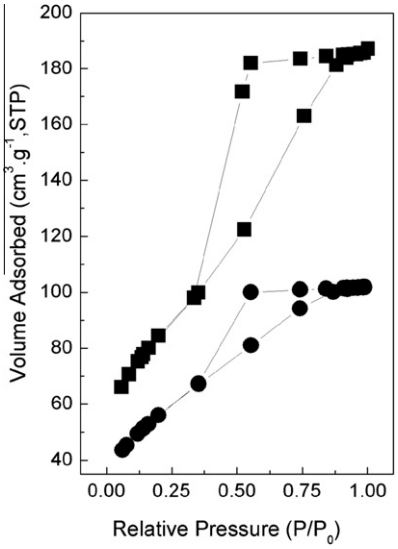

Fig. 2. Nitrogen adsorption–desorption isotherms at 77 K of the Pt-NPs/Al_2O_3 (-■-) and Pt-NPs/CeO_2–Al_2O_3 (-●-) catalysts.

The chemical analysis, S_{BET}, V_p and D_{pore} of the catalysts are summarized in Table 1. The chemical analysis confirmed that both catalysts have similar Pt loadings, around 0.3 wt%. Samples used for XAFS analysis, with 0.6 wt% of Pt loading, showed similar results (data not shown). The N_2 adsorption–desorption isotherms are presented in Fig. 2, showing type IV isotherms according to the IUPAC classification [16], with H2 hysteresis. These results indicate the presence of ink-bottle-shaped mesopores, similar to those observed in the supports [17]. The incorporation of the NPs during the gel formation did not affect the textural properties of the supports (see [17] for comparison). On the other hand, the presence of CeO_2 decreased the S_{BET}, V_p and D_{pore}, with or without the presence of NPs.

XRD patterns of Al_2O_3 and CeO_2–Al_2O_3 xerogels (before calcination), supports and catalysts are shown in Fig. 3a. Both xerogels show a pseudo-boehmite-like structure that is transformed to the γ-Al_2O_3 phase by calcination (Fig. 3a). In the case of the Ce-containing samples, crystalline CeO_2 phase, with bulk fluorite structure, could also be detected (Table 1 and Fig. 3). Interestingly, although the incorporation of the NPs into the gels did not affect significantly the textural properties of the support, the presence of Pt-NPs seems to have helped the crystallization of the ceria phase. This can be seen in Pt-NPs/CeO_2–Al_2O_3 by the better-defined diffraction peaks of the ceria phase (indicated by $*$ in Fig. 3a). The reflections of Pt^0 are not observed at this calcination temperature.

By increasing the calcination temperature to 1073 K (Fig. 3b), the alumina became more crystalline [18]. The apparent crystallite

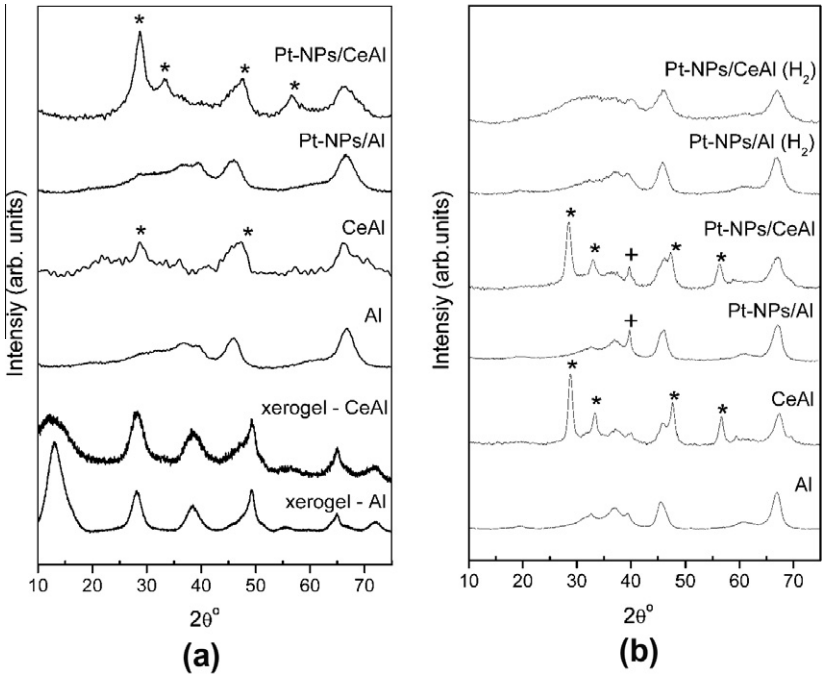

Fig. 3. XRD patterns of samples calcined in air at (a) 773 K and (b) 1073 K. In (a), the XRD patterns of the corresponding xerogels (before calcination) are also shown. The labels are given above each curve (Al = Al_2O_3 and CeAl = CeO_2–Al_2O_3; H_2 = sample treated under H_2, see text for details). * Indicates CeO_2 reflections, and + indicates the (1 1 1) Pt^0 peak.

size of CeO_2 became larger (from 4.0 to 8.2 nm) and, for the Pt-NPs/Al_2O_3 and Pt-NPs/CeO_2–Al_2O_3 catalysts, the main Pt^0 reflection at 39.9° became evident (indicated by + in Fig. 3b). It is interesting to note that a different result was found when the catalysts calcined at 773 K were subsequently treated in H_2 at 1073 K for 8 h (Fig. 3b). The characteristic lines of the CeO_2 fluorite structure disappeared, and the peaks correspondent to Pt^0 are not observed. This is an important result for the POM reaction, which takes place at 1073 K, as it will be discussed below.

The FTIR spectra of adsorbed CO on Pt-NPs/Al_2O_3 and Pt-NPs/CeO_2–Al_2O_3 samples reduced at 773 K are shown in Fig. 4. Both spectra revealed one band at high frequency (HF) ca. 2079 cm^{-1}, assigned to CO linearly bonded to Pt^0 [19]. Interestingly, this band is highly symmetrical and very sharp (FWHM = 23 cm^{-1}) in both catalysts, compared to conventional catalysts prepared by impregnation (FWHM around 50 cm^{-1} and asymmetrical [20]). Given that the FWHM of this band is also sensitive to the size of the Pt clusters, the smaller FWHM indicates a narrower size distribution of the Pt-NPs in the present catalysts. The Pt-NPs/Al_2O_3 also shows two overlapping low-frequency (LF) bands at ca. 1820 and 1767 cm^{-1} (Fig. 4). The band at 1820 cm^{-1} can be assigned to CO bonded to two surface Pt atoms and assigned to CO adsorbed in bridge form [19]. The bands at LF region are strongly suppressed in Ce-containing catalysts.

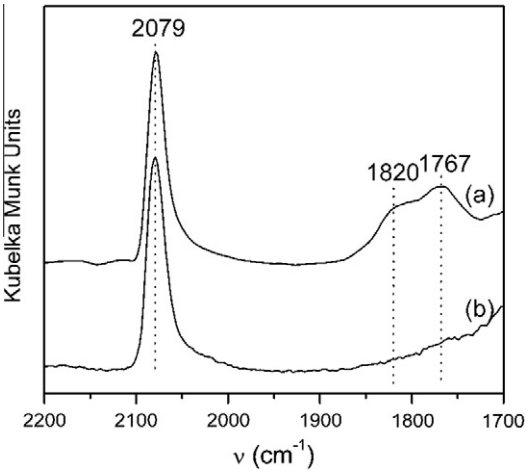

Fig. 4. FTIR spectra of adsorbed CO on (a) Pt-NPs/Al_2O_3 and (b) Pt-NPs/CeO_2–Al_2O_3 catalysts (CO pressure of 10 torr).

TPD-CO profiles in the 2200–1700 cm^{-1} region are shown in Fig. 5A for Pt-NPs/Al_2O_3 and 5B Pt-NPs/CeO_2–Al_2O_3, respectively. The spectra were collected at 298 K after heating the samples to each respective temperature indicated in Fig. 5. The results revealed that the species absorbing at ca. 2076 cm^{-1}, assigned to CO in linear mode, desorbs at temperatures higher than 323 K and shifts to a lower frequency, in both catalysts. The origin of this shift could be a dipole–dipole effect; however, a possible reconstruction of the surface of the Pt particles in the presence of CO at high temperatures cannot be excluded. The Pt-NPs/Al_2O_3 catalyst also shows species absorbing at ca. 1820 cm^{-1} (bridged carbonyls) and 1760 cm^{-1}, both desorbing at around 373 K. Although stretching frequency at 1760 cm^{-1} is fairly rare, it is typically assigned to highly coordinate CO species, probably in threefold bonding sites [21,22].

Fig. 6 shows the XANES spectra (the near edge structure of the XAFS spectra) of the Pt-NPs/Al_2O_3 and Pt-NPs/CeO_2–Al_2O_3 catalysts, compared to the Pt and PtO_2 standards. It can be seen that the two catalysts are similar and their spectra resemble that of metallic Pt. The white lines are slightly more intense in the catalysts spectra than in the Pt standard, suggesting that a small charge transfer might exist with the residual ligand and/or the support. This difference, however, disappears on reducing the catalysts *in situ* at 773 K in H_2.

The EXAFS oscillations and corresponding Fourier transform of the catalysts after *in situ* reduction are shown in Fig. 7. The quantitative analyses are presented in Table 2, and, for comparison, the

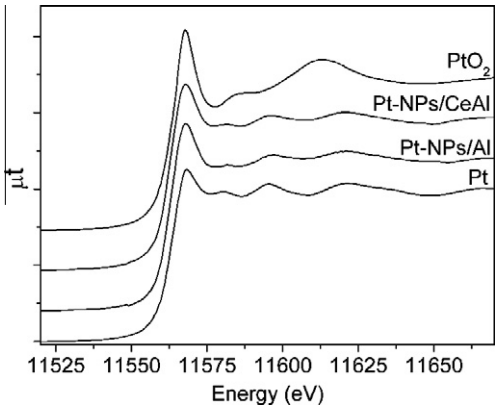

Fig. 6. XANES spectra at Pt L_{III}-edge of the Pt-NPs/Al_2O_3 and Pt-NPs/CeO_2–Al_2O_3 catalysts, compared to Pt and PtO_2 standards.

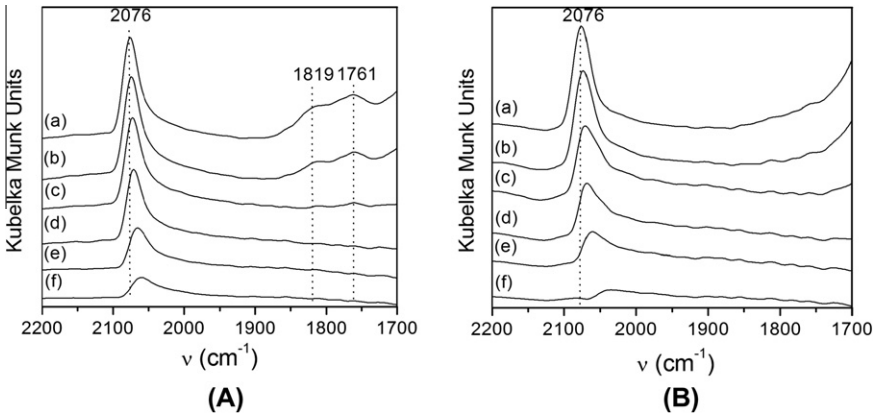

Fig. 5. TPD-CO adsorbed on (A) Pt-NPs/Al_2O_3 and (B) Pt-NPs/CeO_2–Al_2O_3 catalysts previously reduced under H_2 at 773 K (the spectra are taken from CO-saturated surface at 298 K): (a) desorption at room temperature; (b) 323 K; (c) 373 K; (d) 423 K; (e) 473 K; (f) 523 K.

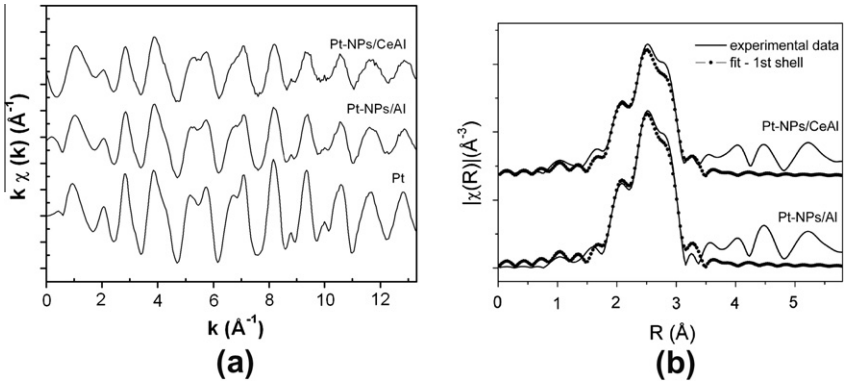

Fig. 7. (a) EXAFS oscillation and (b) corresponding magnitude of the Fourier transform and best fit for the nearest neighbors of Pt-NPs/Al_2O_3 and Pt-NPs/CeO_2–Al_2O_3 catalysts. The samples were reduced flowing H_2 at 773 K, and spectra were collected after cooling at 298 K. In (a), the EXAFS oscillations of the Pt standard (Pt) was shown for comparison.

Table 2
Results from EXAFS analysis of Pt L_{III}-edge for calcined and reduced catalysts.

Catalyst	Shell	1st shell CN	Interatomic distance (Å)	$\Delta\sigma^2$ (Å^2)	ΔE (eV)
Pt foil	Pt–Pt	12	2.765 (5)	0.0054 (1)	6 (1)
Pt-NPs/Al_2O_3[a]	Pt–Pt	6 (1)	2.75 (1)	0.007 (1)	5 (2)
	Pt–O	1.2 (3)	2.00 (2)	0.001 (2)	8 (4)
Pt-NPs/CeO_2–Al_2O_3[a]	Pt–Pt	4 (1)	2.761 (7)	0.006 (1)	6 (1)
	Pt–O	2.0 (3)	1.994 (8)	0.002 (2)	7 (2)
Pt-NPs/Al_2O_3[b]	Pt–Pt	9.1 (8)	2.757 (5)	0.0064 (1)	6 (1)
Pt-NPs/CeO_2–Al_2O_3[b]	Pt–Pt	7.8 (7)	2.755 (5)	0.0067 (5)	6 (1)

[a] Samples calcined in air at 773 K and spectra collected at 298 K.
[b] Samples reduced flowing H_2 at 773 K and spectra collected at 298 K.

results obtained with the catalyst just after calcination are also shown. The best fits for the first coordination shell are shown in Fig. 7b. For both samples, the coordination numbers (CN_{Pt-Pt}) of the Pt–Pt nearest neighbors are reduced compared to bulk, as expected for NPs. For the fresh samples, a small contribution of a Pt–O scattering path has to be included in the fit, in agreement with the XANES results. After *in situ* reduction, there is a slight increase in the CN_{Pt-Pt}, whereas the CN_{Pt-O} contribution disappears. These indicate that residual PVP may have been eliminated [23] with a minor growth of the Pt-NPs. Both catalysts, however, behave in a similar way.

When tested on the dehydrogenation of cyclohexane, the Pt-NPs/Al_2O_3 catalyst showed a slightly larger number of exposed Pt sites (Table 3), consistent with the EXAFS results (Table 2). Considering the catalyst performances, both catalysts are stable with time on stream in the SRM at temperatures around 783 K. The Arrhenius plots for SRM on the Pt-NPs/Al_2O_3 and Pt-NPs/CeO_2–Al_2O_3 catalysts are displayed in Fig. 8. The corresponding E_{app} are reported in Table 3. Both catalysts show a value of E_{app} around 64 kJ mol^{-1}, which agrees with the values previously reported for supported Pt catalysts obtained by impregnation [6,14,18]. On the other hand, the Pt-NPs/CeO_2–Al_2O_3 catalyst has an r_{CH4} twice as high as that of the Pt-NPs/Al_2O_3 catalyst and that cannot be explained by the small difference in Pt-exposed sites on surface. As a consequence, despite the similar E_{app} values for the two catalysts, the TOF_{CH4} value at 783 K is twice higher in the CeO_2-containing catalyst

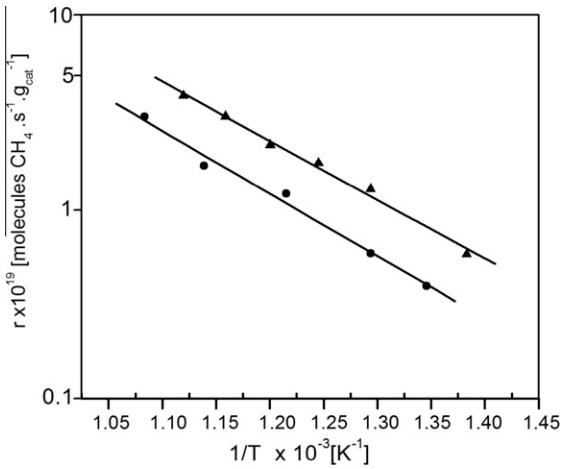

Fig. 8. Arrhenius plot for SRM in Pt-NPs/Al_2O_3 (●) and Pt-NPs/CeO_2–Al_2O_3 (▲) catalysts (feed composition 1:3:0.5 of $CH_4/H_2O/N_2$, with a total flow rate of 2×10^{-2} mol min^{-1}). Temperature ranges from 725 to 925 K.

Table 3
Catalytic data (r_{C6H12}, E_{app}, TOF_{CH4} and r_{CH4}) in the SRM. TOF_{CH4} values were calculated from r_{C6H12}.

Sample	r_{C6H12} (mol g_{cat}^{-1} h^{-1})	r_{CH4} ($\times 10^{-19}$)[a] (mol g_{cat}^{-1} s^{-1})	E_{app} (kJ mol^{-1})	Pt[a] dispersion (%)	TOF $_{CH4}$[b] (s^{-1})
Pt-NPs/Al_2O_3	0.070 ± 0.001	0.688 ± 0.001	65	26	2.7 ± 0.2
Pt-NPs/CeO_2–Al_2O_3	0.065 ± 0.001	1.382 ± 0.001	63	21	4.8 ± 0.2

[a] Pt dispersion calculated from r_{C6H12} at 543 K.
[b] TOF_{CH4} and r_{CH4} were obtained at 783 K.

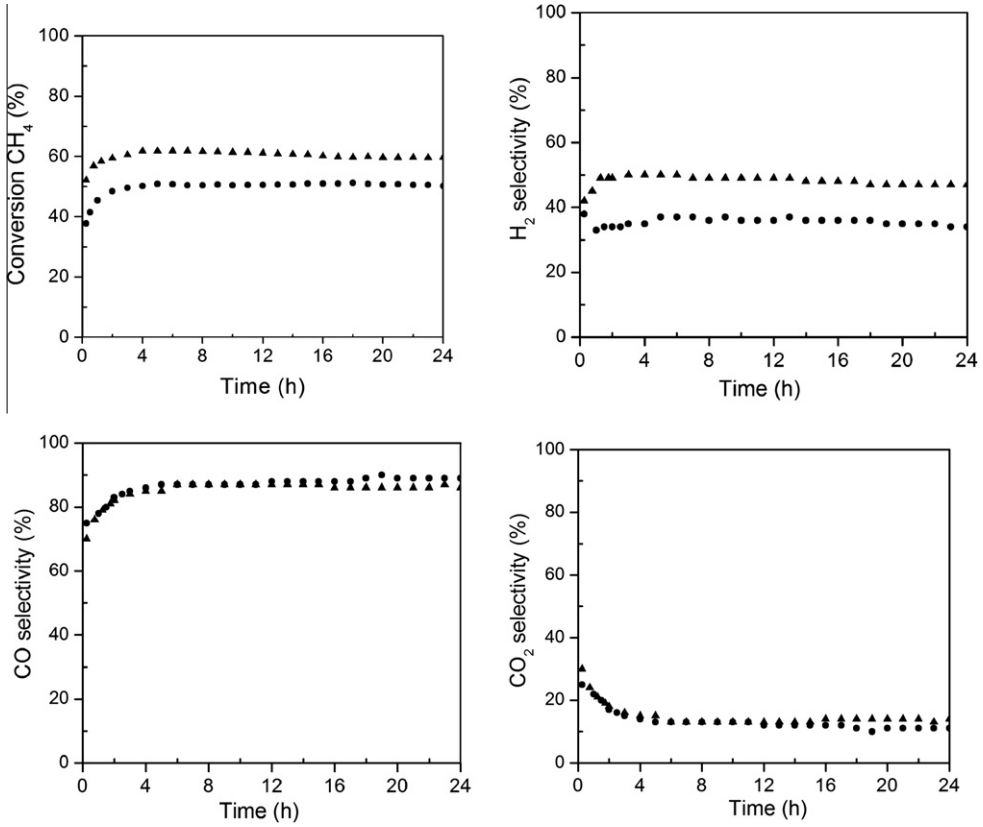

Fig. 9. CH_4 conversion and selectivity to H_2, CO and CO_2 under POM conditions at 1023 K and W/F = 0.4 (g_{cat}^{-1} h mol_{CH4}^{-1}) of the Pt-NPs/Al_2O_3 (●) and Pt-NPs/CeO_2–Al_2O_3 (▲) catalysts (feed composition 2:1:1 of $CH_4/O_2/N_2$).

(Table 3). Related behavior was observed in Pd/$x$$CeO_2$–$Al_2O_3$ and Pt/$x$$CeO_2$–$Al_2O_3$ catalysts prepared by impregnation method, where the increase in Ce loading led to an increase in TOF_{CH4} values [5,6].

The results of the stability tests under POM conditions are shown in Fig. 9. The selectivity to H_2, CO and CO_2 is also plotted against time on stream. In contrast to the SRM, which takes place at 783 K, the Pt-NPs/Al_2O_3 and Pt-NPs/CeO_2–Al_2O_3 catalysts were not initially stable for POM at 1073 K and showed an increase in CH_4 conversion with time on stream. Stability was, however, achieved after about 2 h. Surprisingly, different from what was reported for Pt/Al_2O_3 catalysts obtained by impregnation [5], Pt-NPs/Al_2O_3 catalyst was still stable after 24 h on stream. The stability of Pt-NPs/Al_2O_3 was similar to that of Pt-NPs/CeO_2–Al_2O_3, and no effect of Ce on stability was verified. It is important to note that the H_2/CO ratio was smaller than expected for POM and further studies will be performed to understand the reaction mechanism [24,25].

TEM images of the Pt-NPs/Al_2O_3 and Pt-NPs/CeO_2–Al_2O_3 catalysts used under POM conditions for 24 h are shown in Fig. 10. It seems that the NPs became slightly larger and more faceted (inset in Fig. 10a), but more importantly, they have not formed aggregates in either catalyst.

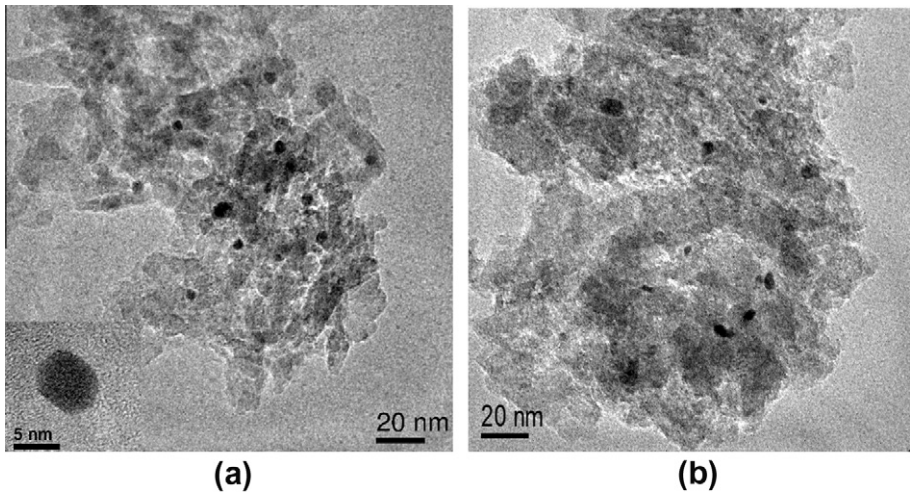

Fig. 10. TEM images of used catalysts under POM conditions at 1073 K for 24 h: (a) Pt-NPs/Al_2O_3 and (b) Pt-NPs/CeO_2–Al_2O_3. Note the Pt-NP faceting shown in the inset.

4. Discussion

The addition of Pt-NPs during sol–gel synthesis of Al_2O_3 and CeO_2–Al_2O_3 successfully resulted in homogeneous solids, in which the Pt-NPs were well dispersed and the textural properties of the supports were not affected. Overall, both samples presented similar behavior in all preparation steps, and as a consequence, the differences in the catalytic behavior due to the support could now be clearly observed.

In fact, since the same batch of colloidal NPs was used to produce the two catalysts, it was expected that Pt-NPs properties would not be responsible for differences in the catalytic properties. EXAFS analysis also pointed out only small differences in the CN_{Pt-Pt} in the reduced samples and similar interatomic Pt–Pt distances. The slightly larger CN_{Pt-Pt} number in the Pt-NPs/Al_2O_3 than in Pt-NPs/CeO_2–Al_2O_3 (9 and 8, respectively) may indicate a change in the morphology during the calcination step, due to differences in wettability of the support. It is worth noting that the average number of 8–9 corresponds to spherical Pt particles of about 2 nm in size, which is smaller than the actual size measured by TEM. More interestingly, in the FTIR of adsorbed CO spectra, the highly symmetrical and sharp (FWHM = 23 cm^{-1}) band observed for each catalyst suggests that the Pt particles is very uniform and shows that the properties of the Pt particles in the catalyst can be controlled when it is obtained from Pt-NPs. On the other hand, the bands in the LF region (at 1819 and 1760 cm^{-1}) are quite different for the Pt-NPs/Al_2O_3 and Pt-NPs/CeO_2–Al_2O_3 catalysts, being strongly suppressed in the Ce-containing catalyst (Pt-NPs/CeO_2–Al_2O_3). The species with a band at 1819 cm^{-1}, assigned to bridge-bonded CO, occurs preferentially at planar Pt sites. The strong suppression of this band in the Pt-NPs/CeO_2–Al_2O_3 catalyst cannot be explained by slight changes in the Pt-NPs morphology suggested by EXAFS but is rather related to geometric effect of CeO_x overlaying the Pt-NPs.

Concerning the electronic properties, the XANES spectra at Pt L_{III}-edge showed similar unoccupied projected density of states of the 5d band for both catalysts, but higher than that for bulk Pt. In this respect, the electron density available for back-donation into the 2π orbital of the CO molecule in the FTIR of adsorbed CO experiments must depend on the Pt particle size. A decrease in Pt particle size leads to a decrease in the C–O bond strength and a lowering of the adsorbed CO band frequency [26]. The position of the band in the HF region assigned to linearly bonded CO is similar in both Pt-NPs/Al_2O_3 and Pt-NPs/CeO_2–Al_2O_3 catalysts, stressing that the electron density on the surface of the Pt is similar as indicated by the XANES data.

Although the number of Pt sites available for dehydrogenation of cyclohexane is slightly higher in the Pt-NPs/Al_2O_3 catalyst (Table 3), the TOF_{CH4} is much lower than in the Pt-NPs/CeO_2–Al_2O_3. These results suggest that in a small cluster, the activity does depend on the support, corroborating previously reported results for Pd/$x$$CeO_2$–$Al_2O_3$ catalysts with various Ce loadings obtained by impregnation [6]. The FTIR results show that the adsorption of CO in the bridged form is suppressed in Pt-NPs/CeO_2–Al_2O_3 (Fig. 4), considering that the Pt-NPs/Al_2O_3 and Pt-NPs/CeO_2–Al_2O_3 samples were prepared from Pt-NPs of same size and the electron density of Pt is similar in both catalysts. Thus, the effect CeO_x overlaying the Pt particles [20] may have caused a loss of terrace sites and by steric consideration suppressed the formation of bridged CO.

It has been demonstrated that the rate of activation of CH_4 on CeO_2 is slower than on a Pt^0 surface [27], and it is accepted that CH_4 is mainly activated on the metal surface [4,28]. On the other hand, Wang et al. [29] proposed a cyclic mechanism of redox couples on Rh–CeO_2/Al_2O_3 catalyst and stated that the coexistence of Ce^{4+}/Ce^{3+} and $Rh^0/Rh^{\delta+}$ redox couples facilitated the activation of CH_4. For CH_4 activation, the electron-deficient state of the Pd^0–$Pd^{\delta+}$ species results in a higher ability to accept ρ electrons from CH_4, thus promoting CH_4 adsorption and C–H bond cleavage [30]. Adopting the reaction mechanism proposed for SRM from DTF results [31], CH_4 decomposes to chemisorbed carbon (C^*) via a pyrolytic mechanism. The active carbon can be removed by reaction with oxygen bound on the surface (O^*), producing CO. The free energy diagrams for Ni and Ru and for Ni at different temperatures indicate that the CH_4 activation became dominant over the CO step with the increase in the temperature [2]. Given that (i) under our reaction condition for SRM, the temperature was low (753–783 K) and (ii) Pd and Pt show higher free energies for O^* than other metals, we might expect lower O^* concentration on Pd and Pt. Either factor can be contributing for increasing concentrations of C^* on Pt surface. C^* can accumulate on the metal surface until the relative rates of the activation of CH_4 and the removal of carbon by formation of CO are balanced. As previously reported [5,6], the $[CePd_xO]Pd^0$ or $[CePt_xO]Pt^0$ adducts formed on the metal surface may be oxidized by H_2O or CO_2 transferring O^* that oxidize the C^* deposited on the metal surface. This oxidation restore the $[CePt_xO]Pt^0$-like species and the metal site. Consequently, the ceria support that has a high capacity to transfer O^* results in the higher oxidation rate of C^* deposited on the Pt surface, which leads to a higher accessibility of the active sites for CH_4 and consequently to higher TOF_{CH4}.

The stability tests of the Pt-NPs/Al_2O_3 and Pt-NPs/CeO_2–Al_2O_3 catalysts under POM conditions showed an increase in activity within the first two hours on stream. The XRD results (Fig. 3) revealed that the Pt-NPs sintered in both Pt-NPs/Al_2O_3 and Pt-NPs/CeO_2–Al_2O_3 catalysts and the supports became more crystalline when calcined in air at the high temperature (1073 K). They were, however, stable in reducing atmosphere. The tendency of Pt agglomerate under oxidizing condition is related to the formation of PtO_x volatile species that have higher diffusivity at this temperature, and Pt sintering occurs mainly by the mechanism of Ostwald ripening [32,33]. As shown by *in situ* XANES [5], under POM conditions, the Pt-NPs were reduced. Thus, to avoid the sintering before the reaction, the catalysts were calcined at a lower temperature (773 K) than the temperature used for the stability test (1073 K). From these results and by the fact that the initial increase in activity with time on stream was similar for both catalysts, the differences in activity might be mainly associated with changes in the textural properties of the support. In fact, the type of atmosphere also seems to affect the Ce phase in the Pt-NPs/CeO_2–Al_2O_3 catalyst. The reducing condition at 1023 K seems to transform the CeO_2 crystalline phase to an amorphous CeO_x phase, as shown by XRD.

After the initial period of stabilization under POM conditions, the Pt-NPs/CeO_2–Al_2O_3 catalyst showed higher activity than Pt-NPs/Al_2O_3, demonstrating the higher reforming activity of Ce-containing catalysts. Interestingly, both Pt-NPs/Al_2O_3 and Pt-NPs/CeO_2–Al_2O_3 catalysts were stable in POM (Fig. 9), and no effect of the support on the stability was detected. In a previous work [5], we have shown stability results on stream for POM on Pt/γ-Al_2O_3 obtained by impregnation. In that case, the conventional Pt/γ-Al_2O_3 catalyst deactivated with time on stream under similar conditions to the ones used in this work, whereas the corresponding conventional Pt/CeO_2–Al_2O_3 catalyst was quite stable. Two mechanisms have been proposed for the sintering of Pt particles: Ostwald ripening, and particle migration and coalescence (PMC) [32]. Under Ostwald ripening, the driving force for sintering comes from the higher chemical potential of the metal atoms in small particles. This driving force may not be favored in the Pt-NPs, which exhibit a narrow size distribution.

For the conventional Pt/γ-Al_2O_3 obtained by impregnation on commercial alumina, TEM images confirmed its low thermal stability by showing extensive Pt sintering and changes in the support morphology [5]. On the other hand, for γ-Al_2O_3 support obtained

by the sol–gel method, Pt sintering was less evident and the support showed higher thermal stability [18]. These results suggest that Pt sintering by PMC is suppressed by the thermal stability of the γ-Al_2O_3 support and Pt particle size. The lack of a Pt–O scattering contribution to the EXAFS signal after reduction also suggests that the Pt-NPs clusters are anchored at supporting oxygen vacancy sites. Both mechanisms, Ostwald ripening and PMC, seem to be suppressed by the thermal stability of γ-Al_2O_3 and the narrow size distribution of the Pt-NPs. This effect has been analyzed in detail and will the subject of a future article.

5. Conclusions

A new strategy was successful in synthesizing Pt clusters of uniform size supported on mixed oxides. The design of catalysts with Pt particles of similar size on different supports clearly pointed out the important role of the CeO_2 in improving the catalytic activity in SRM. The higher TOF_{CH4} of the CeO_2-containing catalyst, Pt-NPs/CeO_2–Al_2O_3, confirmed the relevance of the Pt site surroundings. The higher activity was ascribed to higher accessibility of the Pt sites to CH_4 on removing C^* from active sites by the transfer of O^* from CeO_2 to metal, promoting oxidation of C^*. Pt-NPs showed high thermal stability, and both Pt-NPs/Al_2O_3 and Pt-NPs/CeO_2–Al_2O_3 catalysts were stable under POM reaction condition.

Acknowledgments

The authors are grateful for the financial support of FAPESP (Fundação para o Amparo à Pesquisa do Estado de São Paulo) and CNPq (Conselho Nacional de Desenvolvimento Científico e Tecnológico). LNLS is acknowledged for the access to the TEM-LME and XAFS2 beamline and support.

References

[1] P. Pantu, G.R. Gavalas, Appl. Catal. A 223 (2002) 253.
[2] G. Jones, J.G. Jakobsen, S.S. Shim, J. Kleis, M.P. Andersson, J. Rossmeisl, F. Abild-Pedersen, T. Bligaard, S. Helveg, B. Hinnemann, J.R. Rostrup-Nielsen, Ib Chorkendorff, J. Sehested, J.K. Nørskov, J. Catal. 259 (2008) 147.
[3] Zhi-Pan Liu, P. Hu, J. Am. Chem. Soc. 125 (2003) 1958.
[4] J. Wei, E. Iglesia, J. Phys. Chem. B 108 (2004) 4094.
[5] A.P. Ferreira, D. Zanchet, J.C.S. Araújo, J.W.C. Liberatori, E.F. Souza-Aguiar, F.B. Noronha, J.M.C. Bueno, J. Catal. 263 (2009) 335.
[6] L.S.F. Feio, C.E. Hori, L.V. Mattos, D. Zanchet, F.B. Noronha, J.M.C. Bueno, Appl. Catal. A 348 (2008) 183.
[7] R.A. Van Santen, Acc. Chem. Res. 42 (2009) 57.
[8] P. Wyblatt, Acta Metall. 24 (1976) 1175.
[9] Y. Nagai, T. Hirabayashi, K. Dohmae, N. Takagi, T. Minami, H. Shinjoh, S. Matsumoto, J. Catal. 242 (2006) 103.
[10] G.A. Somorjai, R.M. Rioux, Catal. Today 100 (2005) 201.
[11] T. Teranishi, M. Hosoe, T. Tanaka, M. Miyake, J. Phys. Chem. B 103 (1999) 3827.
[12] A. Guiner, X-ray Diffraction in Crystals, Imperfect Crystals and Amorphous Bodies, Dover Publications Inc., New York, 1994.
[13] N.V. Parizotto, K.O. Rocha, S. Damyanova, F.B. Passos, D. Zanchet, C.M.P. Marques, J.M.C. Bueno, Appl. Catal. A 330 (2007) 12.
[14] A.C.S.F. Santos, S. Damyanova, G.N.R. Teixeira, L.V. Mattos, F.B. Noronha, F.B. Passos, J.M.C. Bueno, Appl. Catal. A: Gen. 290 (2005) 123.
[15] D.C. Koningsberger, B.L. Mojet, G.E. van Dorssen, D.E. Ramaker, Top. Catal. 10 (2000) 143.
[16] K.S.W. Sing, D.H. Everett, R.A.W. Haul, L. Moscou, R.A. Pierotti, J. Rouquerol, T. Siemieniewska, International union of pure and applied chemistry, IUPAC, Pure Appl. Chem. 57 (1985) 603.
[17] R. Rinaldi, U. Schuchardt, J. Catal. 227 (2004) 109.
[18] J.C.S. Araujo, D. Zanchet, R. Rinaldi, U. Schuchardt, C.E. Hori, J.L.G. Fierro, J.M.C. Bueno, Appl. Catal. B 84 (2008) 552.
[19] O. Dulaurent, D. Bianchi, Appl. Catal. A 196 (2000) 271.
[20] B.A. Riguetto, S. Damyanova, G. Gouliev, C.M.P. Marques, A. Petrov, J.M.C. Bueno, J. Phys. Chem. B 108 (2004) 5349.
[21] P.T. Fanson, W.N. Delgass, J. Lauterbach, J. Catal. 204 (2001) 35.
[22] B.E. Hayden, A.M. Bradshaw, Surf. Sci. 125 (1983) 787.
[23] J.H. Kang, L.D. Menard, R.G. Nuzzo, A.I. Frenkel, J. Am. Chem. Soc. 128 (2006) 12068.
[24] D. A Hickmann, L.D. Schmidt, AIChE J. 39 (1993) 1164.
[25] A.P.E. York, T. Xiao, Tian-cun, M.L. Green, J.B. Claridge, Catal. Rev. 49 (2007) 511.
[26] P. Hollins, Surf. Sci. Rep. 16 (1992) 51.
[27] K. Otsuka, Y. Wang, E. Sunada, I. Yamanaka, J. Catal. 175 (1998) 152.
[28] J.H. Bitter, K. Seshan, J.A. Lercher, J. Catal. 176 (1998) 93.
[29] R. Wang, H. Xu, X. Liu, Q. Ge, W. Li, Appl. Catal. A 305 (2006) 204.
[30] G. Zhu, J. Han, D. Yu. Zemlyanov, F.H. Ribeiro, J. Phys. Chem. B 109 (2005) 2331.
[31] H.S. Bengaard, J.K. Nørskov, J. Sehested, B.S. Clausen, L.P. Nielsen, A.M. Molenbroek, J.R. Rostrup-Nielsen, J. Catal. 209 (2002) 365.
[32] A.K. Datye, Q. Xu, K.C. Kharas, J.M. McCarty, Catal. Today 111 (2006) 59.
[33] X. Lai, D.W. Goodmanr, J. Mol. Catal. A: Chem. 162 (2000) 33.